Particle Image Velocimetry in Concentrated Suspensions: Application to Local Rheometry

Frédéric Blanc, Francois Peters, Elisabeth Lemaire

Particle Image Velocimetry in Concentrated Suspensions: Application to Local Rheometry

Frédéric Blanc François Peters Elisabeth Lemaire*

CNRS, Université de Nice, LPMC-UMR 6622, 06108 Nice Cedex 2, France

Abstract

This paper presents an experimental facility that allows simultaneous viscosimetric and Particle Image Velocimetry measurements on concentrated suspensions in a wide-gap Couette rheometer. The experimental procedure is detailed: the optical characteristics of the index-matched suspension are carefully studied, the bottom end effect on both the viscosimetric measurements and the recorded velocity profiles are analysed. First the experimental procedure is tested on a Newtonian fluid whose viscosity is known. The spatial and time resolutions of our device are shown to be 200 μm and 100ms respectively. The precision of the local viscosity measurement is evaluated to better than 4%.

Then we show that the device can be used to characterize the rheological behaviour of a 47%-concentrated suspension of 30 μ m spheres. According to the particles large size, the Brownian motion can be neglected. However, colloidal interaction are still noticeable.

Introduction

The knowledge of the rheological behaviour of concentrated suspensions of solid particles is an important issue since suspensions are involved in many domains like industrial processes or geophysical phenomena. A theoretical understanding of the mechanical behaviour of concentrated suspensions is difficult because of the particle interactions and its experimental characterization is complicated by numerous disturbing effects such as shear induced particle migration or wall slip. During these last decades, a significant effort has been made to develop non-invasive techniques that ensure that the measured properties are actually

*Author to whom all correspondence should be addressed

the bulk properties of the suspensions. Among these techniques, we may cite the Ultrasound Doppler Velocimetry (UDV)[1], the Laser Doppler Velocimetry (LDV)[2][3][4], the Magnetic Resonance Imaging (MRI)[5][6][7], the Particle Tracking Velocimetry (PTV) [8] [9] and the Particle Image Velocimetry (PIV)[10][11][12][13]. UDV use is restricted to rather low concentrated suspensions especially when the particle size is not very small compared to the acoustic wavelength. The MRI is a very powerful technique [14] that allows measuring both the particle concentration and the velocity profiles. Unfortunately, the MRI technique does not allow carrying out the measurements directly inside a commercial viscometer and, usually, the rheological measurements have to be made separately. If one wants to compare simultaneously macroscopic and local rheological measurements, the LDV or PIV techniques are suitable since they are easily implemented on a rheometer but they require to use an index-matched suspension (for a recent review, see [15]). The LDV allows very accurate measurements of the mean and fluctuating parts of the velocity [4] but, since it is a pointwise method, the instantaneous velocity profile cannot be determined. The PIV and PTV are now broadly used techniques in flow measurements [10] but they remain challenging techniques in concentrated heterogeneous media[8][16]. Nevertheless they have been successfully employed to measure velocity fields in concentrated suspensions [11][12][17][18] .

In this paper we describe the PIV facility that we have developed in order to study the rheological behaviour of concentrated suspensions in a wide-gap Couette viscosimeter. We first present the suspension characteristics and detail the experimental device. Then, we validate our experimental procedure with a Newtonian liquid whose viscosity is known and, at last, we present the local rheological measurements performed on a concentrated suspension (Φ=47%).

Transparent concentrated suspension

The suspensions that we study here are composed of monodisperse spherical PMMA particles (manufactured by Microbeads, diameter $31\mu m \pm 4\mu m$, density 1.178) immersed in a mineral oil (manufactured by Cargille, $\eta_0 = 1.03 \pm 0.01$ Pa.s at 34°C) which is Newtonian. We have prepared suspensions of various concentrations between 30% and 50%. The fluid is chosen to match both the the refractive index and density of the particles. At 25°C, its refractive index $n = 1.4900 \pm 0.0005$, its density is 1.18 and its thermal expansion is 3.6 10^{-3}/°C. Thus no sedimentation is observed in the suspensions which are almost transparent, as required by the PIV measurements.

In order to improve the transparency of the suspensions we have to match as closely as possible the refractive index of the particles and of the suspending liquid. This is achieved by controlling the temperature of the suspensions thanks to the Christiansen effect [19][20]. Indeed, the refractive indices of the particles and of the host liquid do not vary in the same way with the temperature. Thus it is possible to improve the index matching at a given wavelength upon varying the temperature. The optimal temperature has been determined by measuring the transmittance of a Φ=50% suspension as a function of the temperature. Figure 1 shows the results obtained with a spectrophotometer (Varian Cary 500). The transmittance is therefore maximum for a temperature T=34°C. All the PIV measurements will be performed at this temperature.

At last, a small amount of the particles (between 0.15% and 0.25%) from the same batch are tagged with a fluorescent dye (Nile Blue A) and serve as PIV-tracers. To dye the particles, we disperse them in a dye-saturated ethanol solution which is heated at 50°C during one hour. The particles are then rinsed in ethanol until the liquid is clear. They are dried and sieved to eliminate possible clusters. The procedure of immersing the particles in ethanol was not found to have any discernible effect on the PMMA particles. Using Scanning Electron Microscopy, we have been able to observe that their size and surface have not been modified.

We have checked that at T=34°C, no sedimentation was observed for several tens of hours. To this purpose, the positions of the fluorescent particles in the laser sheet have been recorded and no displacement was observed.

[Figure 1 about here.]

Description of the flow cell

The rheology of the suspensions is studied in a wide-gap Couette geometry mounted on a controlled-stress rheometer Mars II (Haake). The particles and the fluid are mixed together in the viscosimeter cup which is removable. During the mixing, many air bubbles are trapped in the suspension. They are removed by vacuum degassing after the mixing has stopped. The outer cylinder is then fixed on the reference plane of the rheometer with four screws. The inner cylinder is then slowly moved down until it is located 1 mm above the bottom of the cup. We have chosen such a small distance between the bob and the cup to limit the particle migration from or toward the region situated below the rotor [21]. In turn, we expect to observe significant end effects even though the rotor has been specially designed to reduce the bottom viscous friction. A cavity has been

made in the lower part of the rotor so that an air bubble is trapped between the rotor and the cup and the wall around the bubble has been bevelled (see Figure 2). The inner rotating cylinder ($2R_{in} = 28mm$ in diameter, 60 mm in height) and the outer stationary cup ($2R_{out} = 48mm$ in diameter, 60 mm in height) are made of PMMA, so that their refractive index is approximately matched with the suspension one. The front face has been polished in the form of a rectangular window that lets the laser sheet enter the gap between the cylinders almost without refraction. The inner cylindrical walls have been roughened (except the cup bottom which, on the contrary, has been polished) to minimize the suspension slip.

[Figure 2 about here.]

Description of the experimental device

Figure 3 offers a schematic view of the device. An externally triggered horizontal laser sheet (Lasiris TEC Laser, Stockeryale, 635 nm, 35mW), roughly 100 μm thick, illuminates the transparent suspension located in the wide-gap Couette cell. A camera (PLB 741 U, Pixelink, 1280x1024 pix^2) records successive images of the fluorescent tagged particles. The laser sheet and the camera are fixed on an arc which can be vertically translated. We can thus measure the particles displacement at any height in the suspension.

The laser light excites the dyed tracers which emit isotropically around 650 nm. A high pass filter in front of the camera allows only the fluorescent light to be detected. Thus the scattered and refractive light from the laser is cut off. Linear and tilt stages (Newport) allow positioning the camera and setting the laser sheet horizontally. In order to control the temperature, the device is placed in an isothermal box made of wood covered with 2 cm thick polyurethane sheets. The box is heated by a radiator connected to an heating circulator bath, which is controlled by a Pt 100 resistance thermometer located near the Couette cell. To improve the homogeneity of the temperature in the box, a fan is placed behind the radiator. The temperature is set to 34±0.1°C.

Figure 4 shows a typical picture (inverted contrast) taken 14 mm above the bottom of the cup in a $\phi = 40\%$ suspension.

[Figure 3 about here.]

[Figure 4 about here.]

PIV procedure

The image processing is performed by the open source software DPIVsoft (*https* : *//www.irphe.fr/ meunier/*) developed under Matlab environment. PIV is a technique for measuring velocity fields in a plane. Each image is first divided into overlapping subsets named correlation windows. The cross correlation function of the corresponding windows from two successive images is computed (see Figure 5). The mean displacement in this window is given by the location of the maximum of the cross-correlation function. The same procedure performed on all windows gives the displacement field in the illuminated plane. The FFT-based correlation function algorithm is performed in two steps [22]. A first displacement field is computed, making it possible to compute the local 2D displacement gradient in the suspension. During the second run, the windows are first deformed according to the previously computed displacement gradient, before the definitive displacement field to be determined. The size B of the correlation window for the first run plays an important role in the issue of the velocity field calculation. It should fit two criteria : the number of particles in the window has to be larger than typically 4 and the larger particle displacement should be lower than B/3 [22]. The former is necessary to obtain a sufficiently peaked correlation function, while the latter avoids that too many particles exit the window. The first criterion gives the amount of dyed tracers. A quantity of 0.25% of dyed particles experimentally corresponds to around 5 particles in a B=64 pixels correlation window and allows measurement to be performed high enough above the bottom of the geometry. A larger amount of dyed tracers increases light absorption and degrades the velocity measurement accuracy. The length scale on our image is about 1000 pixels/cm. We can thus rewrite the second criterion evaluated at the inner cylinder surface in terms of rotation speed Ω (in rpm) and frame rate f (in Hz): $\frac{\Omega}{f} \lesssim 10^{-1} rpm.Hz^{-1}$. As the faster rate of our camera is 10Hz, the rotor speed should be smaller than 1 rpm. Finally, we obtain a 60×60 Cartesian velocity field, i.e. a spatial resolution around 200 μm. The time resolution is given by the camera frame rate, at most 10Hz in our case.

[Figure 5 about here.]

Local measurement

Determination of the local shear rate

We calibrate our image plane by fitting two circles to the cylinders surfaces and then find the center of the geometry and the length scale factor from the known gap value. It is thus possible to deduce the velocity components in the cylindrical coordinate system (r, θ), that are then averaged over the azimuthal angle θ. The mean radial velocity is always very close to zero, and the local shear rate is computed from the mean azimuthal velocity $V_\theta(r,t)$ by : $\dot{\gamma}(r) = r\frac{\partial}{\partial r}\frac{V_\theta}{r}$. To avoid numerical fluctuations of the spatial derivative, a function is fitted to the experimental velocity profile $V_\theta(r,t)$:

$$V_{fit}(r) = V_{Newtonian} + f(r) = ar + \frac{b}{r} + \frac{c}{r^2} \tag{1}$$

where a,b and c are free parameters. The shear rate is deduced from the differentiation of the fitting function.

Determination of the local shear stress

In the hypothesis of an infinitely high cylinder, it is possible to deduce the shear stress $\sigma_{r\theta}(r,t)$ from the torque on the rotating cylinder $\Gamma_{inf}(t)$ by

$$\sigma_{r\theta}(r,t) = \frac{\Gamma_{inf}(t)}{2\pi r^2 L} \tag{2}$$

where L is the height of the sheared fluid. This hypothesis does not hold since L is not very large compared to the gap width. A significant bottom end effect exists and has to be accounted for. To this purpose, we perform experiments on the suspending liquid alone. We measure the torque Γ_{total} and the rotor angular velocity Ω for different values of the sheared liquid height. All results are displayed in Figure 6. It shows a linear behaviour for each height L of sheared Newtonian liquid in the gap. This linear behaviour can also be seen in Figure 7 where $\frac{\Gamma_{total}}{\Omega}$ is plotted versus L. In this representation, all data collapse in a single linear curve. We deduce :

$$\frac{\Gamma_{total}}{\Omega} = a_1 L + a_2 \tag{3}$$

with $a_1 = 0.397\ \mu Nm.rpm^{-1}.mm^{-1}$ and $a_2 = 4.44\ \mu Nm.rpm^{-1}$. Γ_{total} is the sum of two terms, $\Gamma_{inf} = a_1 L\Omega$ which corresponds to the torque when $L \to \infty$ and $\Gamma_{bottom} = a_2\Omega$ which can be interpreted as the bottom contribution to the

torque. In particular, we can deduce the viscosity from the value of a_1. Indeed, for a newtonian liquid sheared between two infinite cylinders, the relation between the torque on the inner rotating cylinder and its angular velocity reads:

$$\frac{\Gamma_{inf}}{\Omega L} = \frac{4\pi R_{in}^2 R_{out}^2}{R_{out}^2 - R_{in}^2}\eta \tag{4}$$

From the value of a_1 together with equ. (4), the viscosity is measured to be $\eta_0 = 1.02$ Pa.s.

Concerning the bottom end correction, we can write,

$$\frac{\Gamma_{bottom}}{\Gamma_{total}} = \frac{1}{1 + \dfrac{\Gamma_{inf}}{\Gamma_{bottom}}} = \frac{1}{1 + 8.96 \cdot 10^{-2} L(mm)} \tag{5}$$

In a typical experiment L=50 mm, so $\dfrac{\Gamma_{bottom}}{\Gamma_{total}} = 18.2\%$, meaning that the bottom end influence should not be neglected in this geometry. In the following, this bottom contribution is subtracted from the total torque, in order the shear stress to be computed from equ.(2).

[Figure 6 about here.]

[Figure 7 about here.]

Validation of the procedure

First we want to check the validity of the local PIV measurement for a Newtonian liquid, namely the host liquid of the suspension. It is seeded with some fluorescent PMMA particles (2a=31μm) that amount to 0.25% of the total volume. Figure 8 shows the azimuthal velocity profile in the gap at different heights z above the bottom of the outer cylinder in the pure suspending liquid. The velocity is normalized by the inner cylinder velocity. The experimental data (symbols) are compared to finite element (f.e.m.) computations performed by Comsol Software (solid lines), and to the expected Newtonian flow profile between infinite cylinders (dashed line). This last (non-normalized) profile has the well known expression:

$$V_{inf} = \Omega\left(\frac{R_{in}^2 R_{out}^2}{R_{out}^2 - R_{in}^2}\frac{1}{r} - \frac{R_{in}^2}{R_{out}^2 - R_{in}^2} r\right) \tag{6}$$

and the corresponding shear rate is given by:

$$|\dot{\gamma}| = 2\Omega \frac{R_{in}^2 R_{out}^2}{R_{out}^2 - R_{in}^2} \frac{1}{r^2} \tag{7}$$

Experimental and numerical data are in very good agreement. As expected, the end effect is noticeable up to an height of $z \simeq 10mm$, which is the gap width. This is obviously the origin of the bottom end effect displayed in Figure 6 and 7. Above 10 mm, the relative discrepancy from a Newtonian profile calculated for infinite cylinders is less than 4%.

[Figure 8 about here.]

The normalized velocity profile measured at a height z=14mm above the bottom is plotted on Figure 9. The height of liquid in the gap is h=26.4mm (the sum of L=25.4 mm and 1mm which is the distance between the bob and the cup). Also displayed is the fitting function, equ.(1), and the infinite cylinder theoretical profile, equ.(6). The shear rate profile from the velocity fit is shown on Figure 10 together with the expected profile from equ.(7). Again the agreement is very good. The viscosity profile calculated from one single shear rate profile $\eta(r) = \dfrac{\sigma(r)}{\dot{\gamma}(r)}$, that is displayed on Figure 11, is clearly characteristic of a Newtonian liquid. The dashed lines take into account the standard error calculated from 80 profiles. The overall mean viscosity value $\eta_{micro} = 1.07 \pm 0.01\, Pa.s$ is in good agreement with the value $\eta_0 = 1.02$Pa.s that has been deduced from the macroscopic measurement shown in the previous section. Furthermore, both values are consistent with the measurement carried out with the Mars II equipped with a narrow-gap cylinder geometry Z20 DIN Ti, $\eta_0 = 1.03 \pm 0.01$ Pa.s.

[Figure 9 about here.]

[Figure 10 about here.]

[Figure 11 about here.]

Viscous behaviour of a 47% concentrated suspension

Now that we have validated the experimental apparatus for pure liquid measurements, we test it in the field of concentrated suspensions. We mainly perform local measurements on a ϕ =47% suspension. This volume fraction seems at first sight moderate. Actually, as it will appear below, the packing fraction ϕ^* of our suspensions is around 0.53, and not 0.61-0.63 as usual, so that $\phi \sim 0.9\phi^*$.

First, we have measured the flow curve of the suspension in a narrow-gap Couette cell Z20 DIN Ti (inner radius 10 mm, outer radius 10.85 mm) in the range $2\ 10^{-2}s^{-1} < \dot{\gamma} < 2.5s^{-1}$. It fits well to a power law:

$$\sigma_{r\theta} = 40\ \dot{\gamma}^{0.875} \tag{8}$$

This slight shear-thinning behaviour is classically observed in such non-brownian suspensions and the value of the exponent is consistent with that found by Gadala-Maria and Acrivos [23] or by Narumi et al .[24].

Concerning the local measurements, we have performed the same experiment as in the case of the pure suspending liquid to check the influence of the vertical position on the velocity profile. The results are shown in Figure 12. As in the previous section, the bottom influence on the velocity profiles is negligible above 10 mm. In the following, all local measurements are performed 14mm above the bottom.

The measurement of the suspension viscosity are performed just after the shear flow has begun without any pre-shear. Thus no or very weak migration is expected to have occurred. Nevertheless, since there is no real consensus about the characteristic time of the shear-induced migration, the assumption of a homogeneous suspension has to be checked. To this purpose, we have measured the time evolution of the instantaneous velocity at different locations in the gap. As it can be seen in Figure 13, after a transient decrease, the velocity stabilizes to a plateau value and does not change anymore at the time scale of our experiment. Such a transient has already been related in previous papers [23][25] and is supposed to be due to the formation of a shear-induced microstructure[23]. In particular, Gadala-Maria and Acrivos [23] showed that the steady viscosity is reached after a characteristic strain of about 1. This is consistent with our measurements: taking $V_m = 1cm.s^{-1}$ for the mean bob velocity during the transient, and $\tau = 10s$ for the typical transient time, we deduce the characteristic strain $\gamma = V_m\tau/(R_{out} - R_{in}) \sim 1$. The velocity profiles that are presented in the following are the result of a time average over approximately 12s once the plateau has been reached. Thus no significant migration is expected to take place at the time scale of one experiment. It should be stressed that at longer times, a significant variation of the velocity is measured, which should be related to a change in the particle concentration profile. The velocity change is typically 1% per revolution of the bob. However, in the experiments reported in this paper, a suspension was never sheared for more than 4 revolutions before it was completely mixed again, so that it can be considered homogeneous.

We have measured the velocity profiles for the ϕ =47% suspension for several values of the torque applied on the bob. The bob angular velocity was also recorded. Since the constitutive law of the suspension has been determined as a power law, we expect the normalized velocity profiles $v_\theta/\Omega R_{in}$ obtained for different torques to collapse onto a single curve:

$$\frac{V_\theta}{\Omega R_{in}} = \frac{(\frac{R_{out}}{r})^{\frac{m}{2-m}} - \frac{r}{R_{out}}}{(\frac{R_{out}}{R_{in}})^{\frac{m}{2-m}} - \frac{R_{in}}{R_{out}}} \tag{9}$$

This is observed in Figure (14) where the normalized velocity profiles obtained for the torque values $\Gamma = 100, 250, 500, 700\mu$Nm are displayed.

The experimental normalized velocity profile measured for a torque Γ = 500μNm is displayed on Figure (15) together with the expected profile from the law (8). For comparison, the Newtonian profile has also been plotted. The agreement is fairly good, except close to the inner and outer cylinders. The discrepancy observed near the outer cylinder originates in the fact that the PIV software can not measure displacements smaller than approximately 0.5 pixel, due to the middling quality of the images and to the small number of particles in a correlation window. In addition, near the inner cylinder, the first two velocity values are underestimated due to the overlapping of the correlation windows with the inner cylinder that lacks tracers. As a consequence, our PIV device does not allow for an accurate determination of the wall slip.

From the velocity profile, the viscosity profile is computed and compared to the expected profile from Eqs. (2), (5) and (8) on Figure 16. Since no significant migration has occurred during the experiment time, and since the viscosity variation across the gap is weak, the bottom end correction (5) which has been determined for a newtonian fluid should be still valid. The agreement is quite good again, especially if we keep in mind that macroscopic rheometric measurements suffer some uncertainty. Measuring the absolute viscosity of a liquid with a precision higher than a few percents is a hard task. The case of concentrated suspensions is even more tricky due to a possible wall slip at the interface between the suspension and the container. As shown on Figure 16, a minute change in the parameter k substantially reduces the 5 % gap between experimental and expected profiles. By the way, the PIV bulk measurement of the viscosity is not altered by the wall slip, except near the walls.

Finally, we measure the viscosity profile of the suspension for different values of the solid volume fraction. The mean shear rate was kept approximately constant whatever the volume fraction by adjusting the torque on the bob in

such a way that $\Omega \sim 0.4$rpm, resulting in $\dot{\gamma} \sim 5.10^{-2}\mathrm{s}^{-1}$. Figure (17) displays the relative viscosity measured at the position $r/R_{out} = 0.77$ as a function of the solid volume fraction. The experimental points are fitted to a Maron-Pierce law [26]:

$$\frac{\eta}{\eta_0} = \frac{1}{\left(1 - \frac{\Phi}{\Phi^*}\right)^2} \tag{10}$$

which gives the packing volume fraction $\Phi^* = 0.534$. This seems lower than the usual values measured for non-colloidal suspensions around 0.6. We conjecture some residual colloidal interactions between the particles. As a consequence, the volume fraction that we chose for most of the local measurements displayed in this paper, namely $\Phi = 0.47$, corresponds to a fairly concentrated suspension. We can note the exponent 2 in equ.(10) is well appropriate to our experimental data. However, more experimental points, in particular close to ϕ^*, would be necessary to be more conclusive.

[Figure 12 about here.]

[Figure 13 about here.]

[Figure 14 about here.]

[Figure 15 about here.]

[Figure 16 about here.]

[Figure 17 about here.]

Conclusion

We have presented an experimental protocol that allows for determining simultaneously the macroscopic and the local rheological properties of a concentrated suspension. A ϕ=47% suspension is sheared in a wide-gap Couette cell ($R_{in} = 14mm$ and $R_{out} = 24mm$) mounted on controlled shear stress rheometer. The average viscosity of the suspension is determined from the variation of the rotor spin rate with the applied torque while the local viscosity is deduced from the PIV measurement of the velocity profile in the flowing suspension together with the torque data. The PIV measurement in such a concentrated suspension has been made possible by a close index-matching of the particles and host liquid, that allows to record satisfactory images 1.5 cm deep in the suspension.

First we have checked the validity of the experimental procedure with a Newtonian simple liquid. The influence of the bottom end on both the velocity profiles and the macroscopic measurements has been carefully studied. Upon varying the liquid height, the torque correction that is to be introduced to account for the bottom friction has been determined. The bottom end effect on the velocity profiles has been analysed upon measuring the flow profiles at different positions above the cup bottom. We noted that above roughly 10 mm, i.e. the gap thickness, the velocity profiles only slightly depend on the vertical position. The local viscosity can be deduced from the velocity profiles measured at heights larger than 10 mm together with the torque data, corrected for the bottom end effect. Its value agrees within 4% with the macroscopic viscosity. The spatial and time resolution for the determination of the velocity profiles have been evaluated to respectively 200 μm and 100 ms, and the statistical precision of the viscosity measurement, about 1%.

Once the procedure had been checked with a Newtonian liquid, local measurements on concentrated suspensions have been performed. We have been able to measure viscosity profiles over the 1cm gap with a 4 % statistical resolution. These local measurements are in good agreement with the macroscopic measurements. In particular, the shear-thinning behaviour of the suspension evidenced by the macroscopic flow curve has been observed and the expected 10% variation of the viscosity over the gap has been measured.

The experimental facility that we have presented here allows to measure the variation of the viscosity with the particle concentration. Since the divergence law of the viscosity near the packing volume fraction is still an open problem, we plan to perform some more measurements in this concentration range.

Finally, one difficult but interesting and open problem that arises in such measurements of suspension properties in a wide-gap Couette cell is the shear-induced migration (for a recent review, see [27]). Thanks to the good time resolution of our apparatus, we have been able to check that the migration was sufficiently slow in our case to induce only weak variations of the velocity profiles at the time scale of one experiment. However, we clearly understand that the main drawback of our experimental device is the lack of a quantitative concentration profile measurement, that will be necessary in order to deal with the open question of the shear-induced migration models [28][29][30][31][32]. At this time, we were not able to measure concentration profiles due to the large uncertainties linked with the small concentration of tracers, but some experiments are in progress, with particles larger than the laser sheet thickness, where we try to slightly tag the host liquid in place of some tracer particles.

Acknowledgments

This work was supported by the Agence Nationale pour la Recherche (Program ANR-08-BLAN-0048-CSD 2). We are grateful to Laurent Lobry for his help with f.e.m. computations and Laurence Bergougnoux for helpful discussions concerning PIV.

References

[1] Manneville S, Bécu L, Colin A: High-frequency ultrasonic speckle velocimetry in sheared complex fluids, Eur. Phys. J. App. Phys. 28(3) (2004) 361–373.

[2] Muller S: Velocity measurements in complex flows of non-newtonian fluids, Korea-Aust. Rheo. J. 14 (2002) 93–105.

[3] Jana S, Kapoor B, Acrivos A: Apparent wall slip velocity coefficients in concentrated suspensions of noncolloidal particles, J. Rheol. 39 (1995) 1123.

[4] Shapley N, Armstrong R, Brown R: Laser doppler velocimetry measurements of particle velocity fluctuations in a concentrated suspension, J. Rheol. 46 (2002) 241.

[5] Abbott J, Tetlow N, Graham A, Altobelli S, Fukushima E, Mondy L, Stephens T: Experimental observations of particle migration in concentrated suspensions: Couette flow, J. Rheol. 35 (1991) 773.

[6] Raynaud J, Moucheront P, Baudez J, Bertrand F, Guilbaud J, Coussot P: Direct determination by nuclear magnetic resonance of the thixotropic and yielding behavior of suspensions, J. Rheol. 46 (2002) 709.

[7] Ovarlez G, Bertrand F, Rodts S: Local determination of the constitutive law of a dense suspension of noncolloidal particles through magnetic resonance imaging, J. Rheol. 50 (2006) 259.

[8] Breedveld V, van den Ende D, Bosscher M, Jongschaap R, Mellema J: Measurement of the full shear-induced self-diffusion tensor of noncolloidal suspensions, J. Chem. Phys. 116 (2002) 10529.

[9] Nicolai H, Herzhaft B, Hinch E, Oger L, Guazzelli E: Particle velocity fluctuations and hydrodynamic self-diffusion of sedimenting non-brownian spheres, Phys. Fluids 7 (1995) 12.

[10] Adrian R: Twenty years of particle image velocimetry, Exp. Fluids 39(2) (2005) 159–169.

[11] Lenoble M, Snabre P, Pouligny B: The flow of a very concentrated slurry in a parallel-plate device: Influence of gravity, Phys. Fluids 17 (2005) 073303.

[12] Wiederseiner S, Ancey C, Rentschler M, Andreini N: Rheophysics of highly concentrated coarse-particle suspensions in a wide-gap couette rheometer, AIP Conference Proceedings 1145 (2009) 1063.

[13] Zachos A, Kaiser M, Merzkirch W: Piv measurements in multiphase flow with nominally high concentration of the solid phase, Exp. Fluids 20(3) (1996) 229–231.

[14] Huang N, Ovarlez G, Bertrand F, Rodts S, Coussot P, Bonn D: Flow of wet granular materials, Phys. Rev. Lett. 94(2) (2005) 4.

[15] Wiederseiner S, Andreini N, Epely-Chauvin G, Ancey C: Refractive-index and density matching in concentrated particle suspensions: a review. To be published in Exp. Fluids.

[16] Hassan Y, Dominguez-Ontiveros E: Flow visualization in a pebble bed reactor experiment using piv and refractive index matching techniques, Nucl. Eng. and Des. 238(11) (2008) 3080–3085.

[17] Lenoble M: Écoulement et ségrégation dans des pâtes granulaires modèle, Ph.D. thesis, Université Bordeaux I (2005).

[18] Wiederseiner S: Rheophysics of Concentrated Particle Suspensions in a Couette Cell using a Refractive Index Matching Technique, Ph.D. thesis, Ecole Polytechnique Fédérale de Lausanne (2010).

[19] Christiansen C: Untersuchungen über die optischen eigenschaften von fein vertheilten körpern, Ann. Phys. 439 (1885) 298.

[20] Christiansen C: Untersuchungen über die optischen eigenschaften von fein vertheilten körpern, Ann. Phys. 259 (1884) 298.

[21] Leighton D, Acrivos A: The shear-induced migration of particles in concentrated suspensions, J. Fluid Mech. 181 (2006) 415–439.

[22] Meunier P, Leweke T: Analysis and treatment of errors due to high velocity gradients in particle image velocimetry, Exp. Fluids 35(5) (2003) 408–421.

[23] Gadala-Maria F, Acrivos A: Shear-induced structure in a concentrated suspension of solid spheres, J. Rheol. 24 (1980) 799.

[24] Narumi T, See H, Suzuki A, Hasegawa T: Response of concentrated suspensions under large amplitude oscillatory shear flow, J. Rheol. 49 (2005) 71.

[25] Narumi T, See H, Honma Y, Hasegawa T, Takahashi T, Phan-Thien N: Transient response of concentrated suspensions after shear reversal, J. Rheol. 46 (2002) 295.

[26] Maron S, Pierce P: Application of ree-eyring generalized flow theory to suspensions of spherical particles, J. Coll. Sci. 11 (1956) 80–95.

[27] Morris J F: A review of microstructure in concentrated suspensions and its implications for rheology and bulk flow, Rheol. Acta 48(8) (2009) 909–923.

[28] Phillips R, Armstrong R, Brown R, Graham A: A constitutive equation for concentrated suspensions that accounts for shear-induced particle migration, Phys. Fluids A .

[29] Nott P, Brady J: Pressure-driven flow of suspensions: simulation and theory, J. Fluid Mech. 275 (1994) 157–199.

[30] Mills P, Snabre P: Rheology and structure of concentrated suspensions of hard spheres. shear induced particle migration, J. Phys. II 5(10) (1995) 1597–1608.

[31] Buyevich Y: Particle distribution in suspension shear flow, Chem. Eng. Sci. 51(4) (1996) 635–647.

[32] Morris J, Boulay F: Curvilinear flows of noncolloidal suspensions: The role of normal stresses, J. Rheology 43 (1999) 1213.

List of Figures

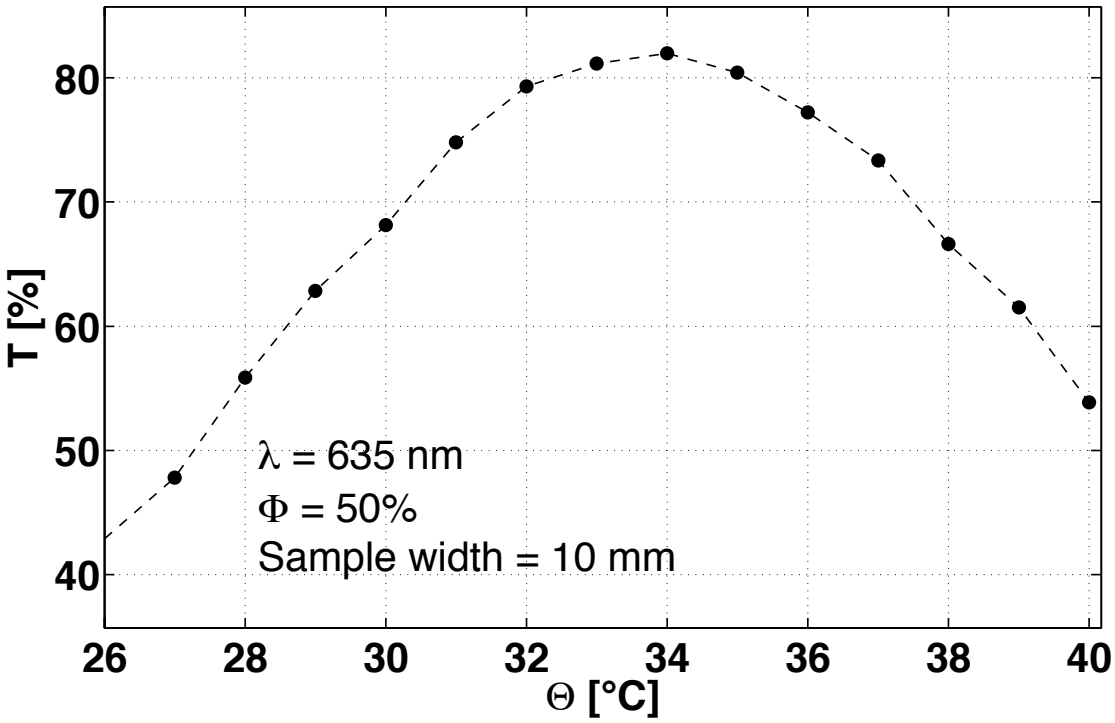

Figure 1: Spectrophotometer measurement of the transmittance of a $\Phi = 50\%$ suspension of 31 μm PMMA particles in Cargille mineral oil versus temperature. The particle liquid index matching is thus found to be optimal for a temperature T= 34°C and λ=635nm

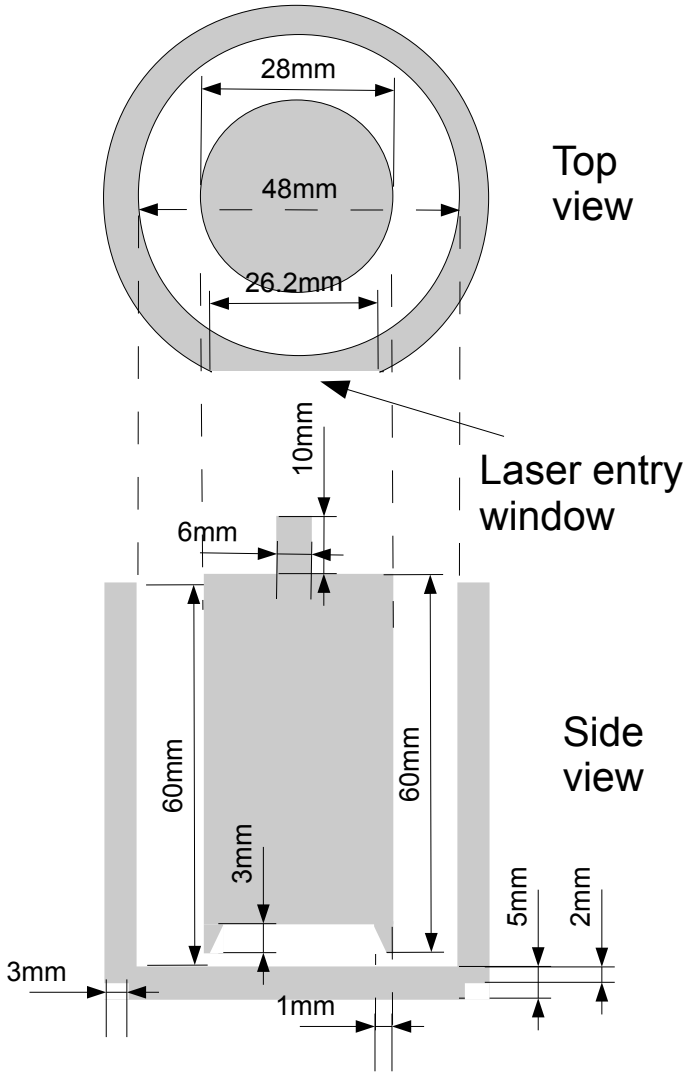

Figure 2: Schematic drawing of the Couette geometry that is used for the PIV measurements. Both cylinders are made of plexiglas. Their surfaces in contact with the suspension have been roughened to minimize wall slip when the suspension is sheared.

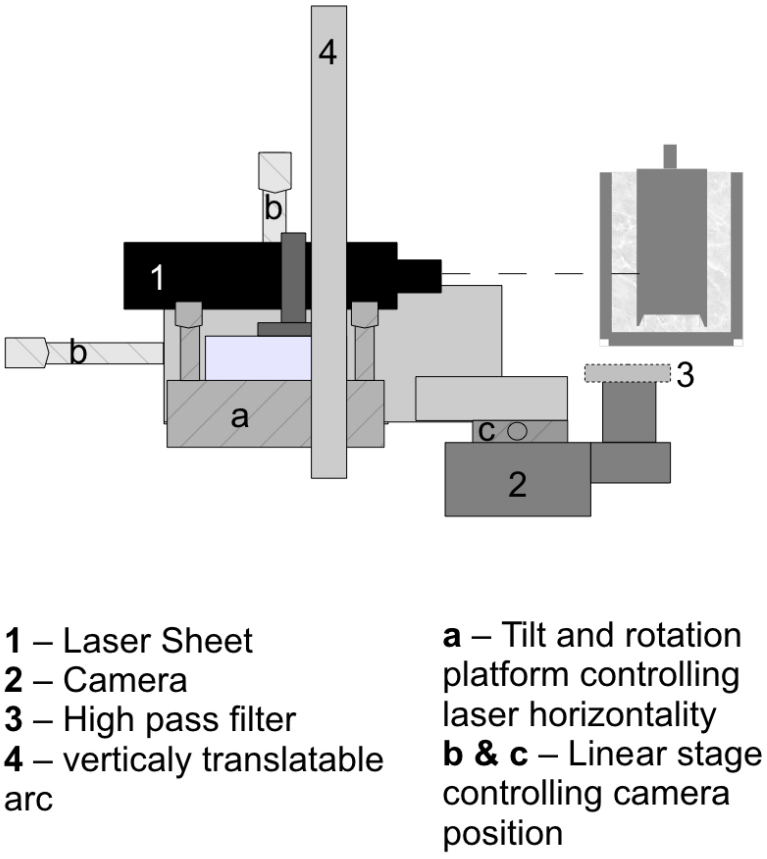

Figure 3: PIV set-up: A laser sheet (Lasiris TEC Laser, Stockeryale, 635 nm, 35mW), roughly 100μm thick, illuminates an horizontal plane of the transparent suspension located in the wide-gap Couette cell. A camera (PLB 741 U, Pixelink, 1280x1024 pix^2) situated under the bottom of the cup records successive images of the fluorescent tagged particles. The laser sheet and the camera are both fixed on an arc which can be vertically translated.

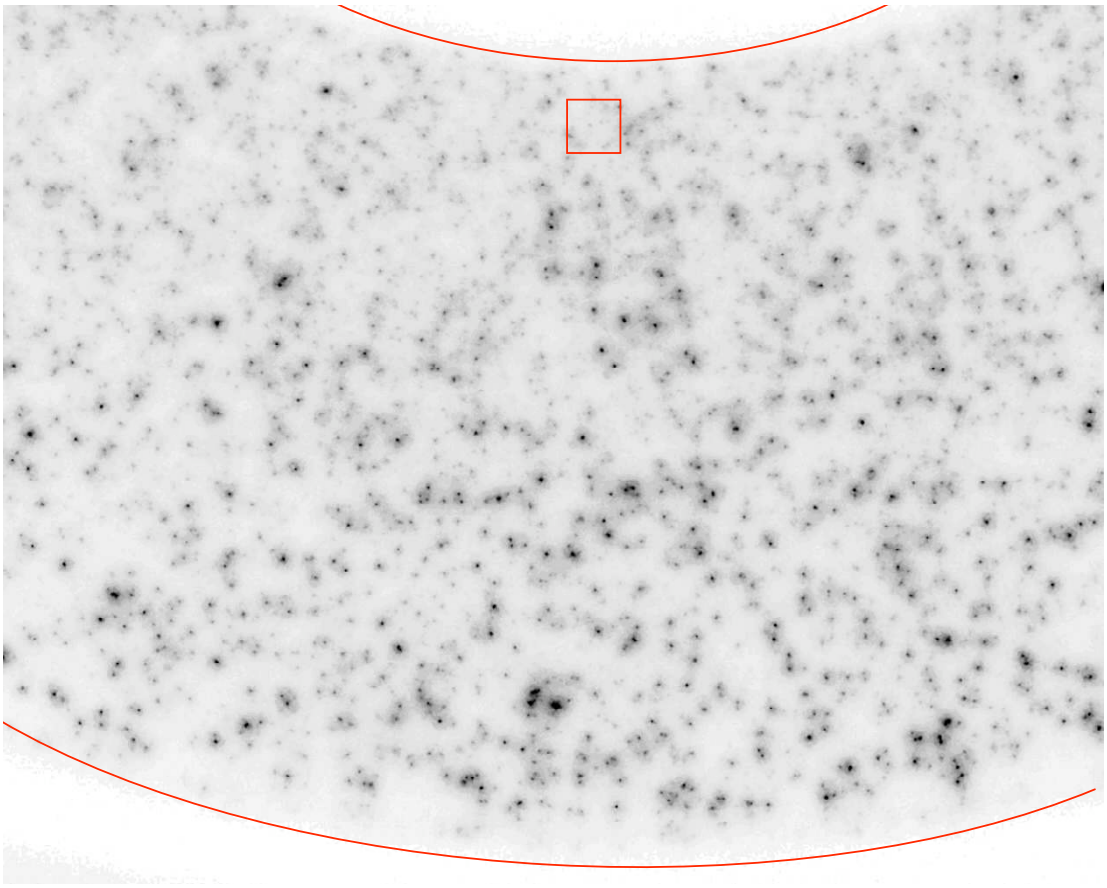

Figure 4: Typical image (inverted contrast) obtained 14 mm from the bottom of the geometry in a 40% suspension - Rotor and stator are fitted with two circles - Square: correlation window

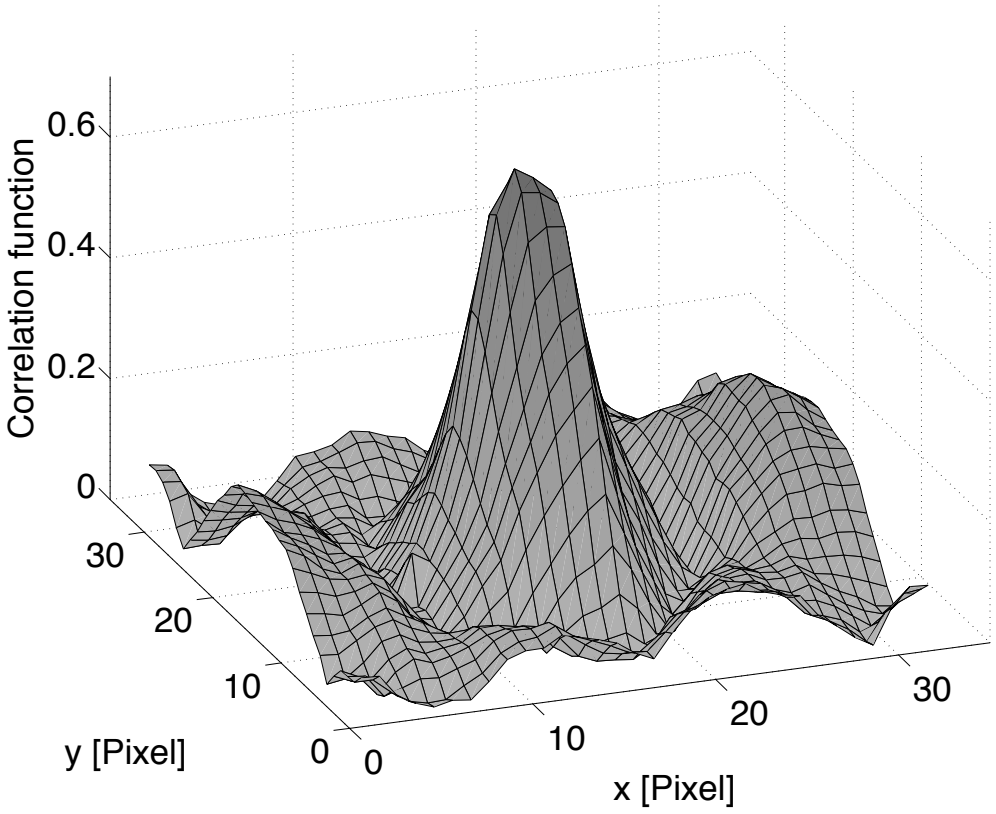

Figure 5: Typical cross-correlation function obtained from our images

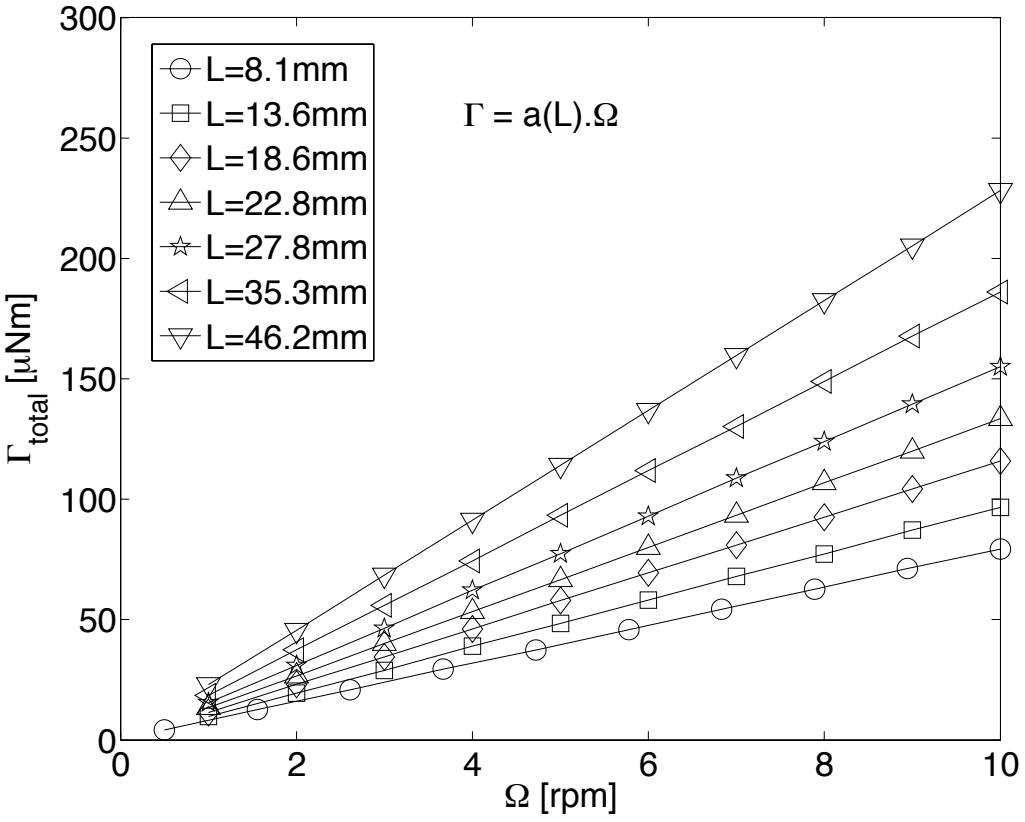

Figure 6: Measured torque vs rotor angular velocity for different heights of the Newtonian liquid

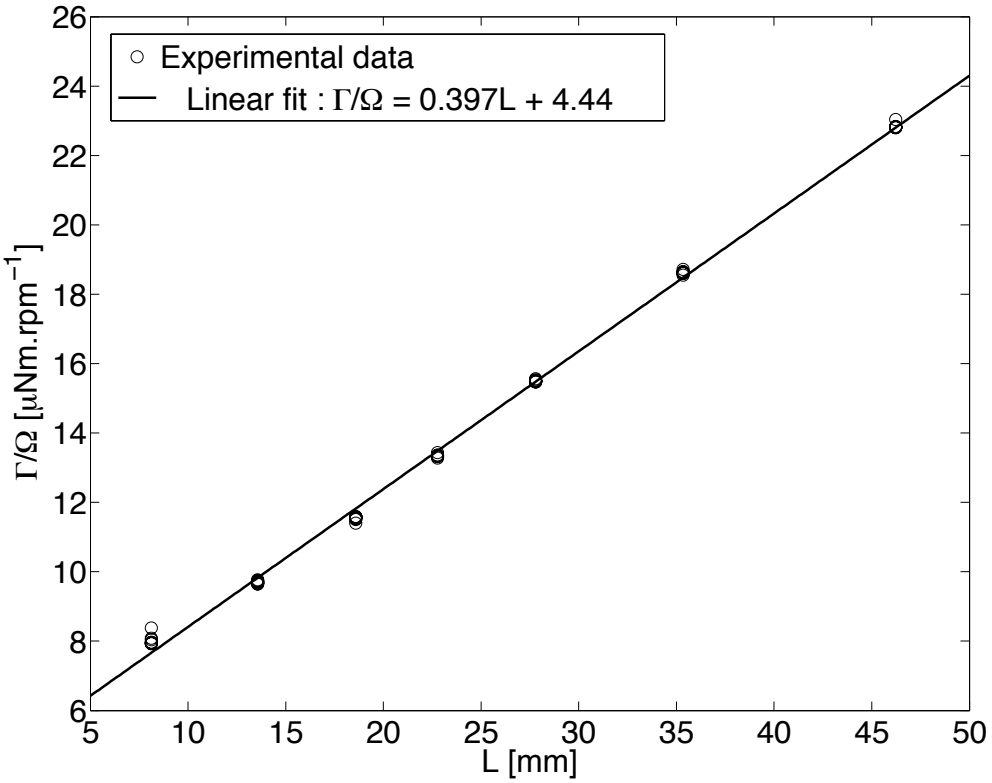

Figure 7: The ratio of the applied torque (in μNm) to the measured bob spin rate (in rpm) is plotted versus the sheared liquid height, L, in the Couette cell gap (in mm). The extrapolation of the curve for h=0 gives the bottom correction that is to be taken into account for the determination of the shear stress in the gap.

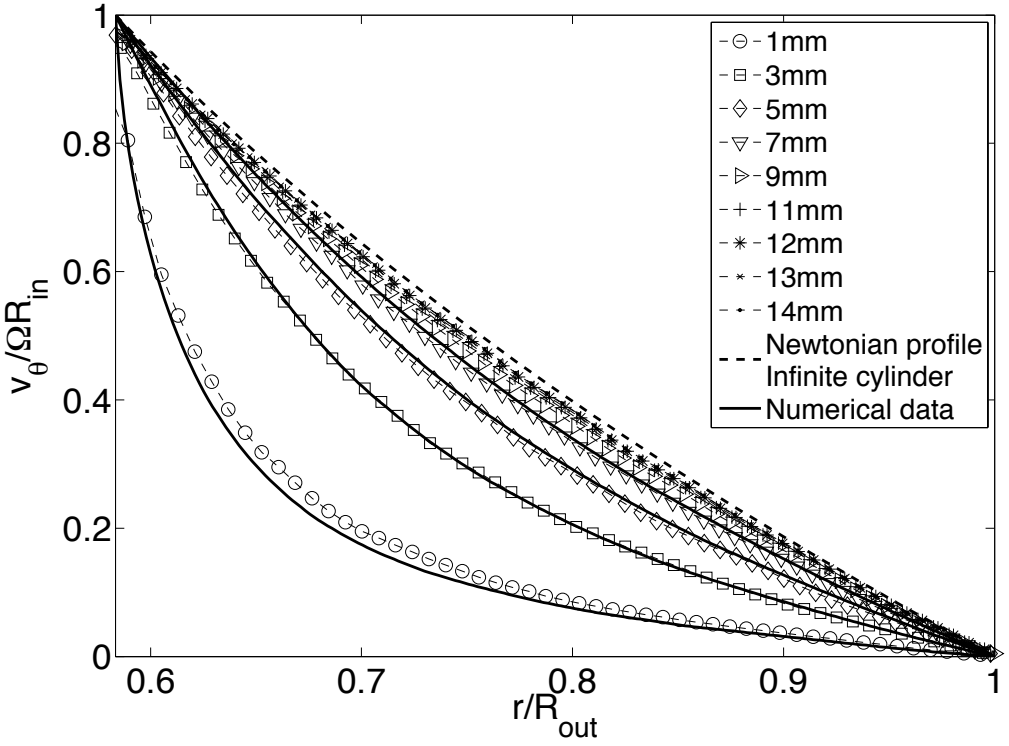

Figure 8: Dimensionless azimuthal velocity profile in the Newtonian liquid. Each profile is the result of an average over 80 instantaneous profiles ($\sim$ 10s). The different profiles are determined at different heights from the bottom of the cup-Symbols: experimental data -Solid lines: f.e.m. numerical data- Dashed line: infinite cylinder.

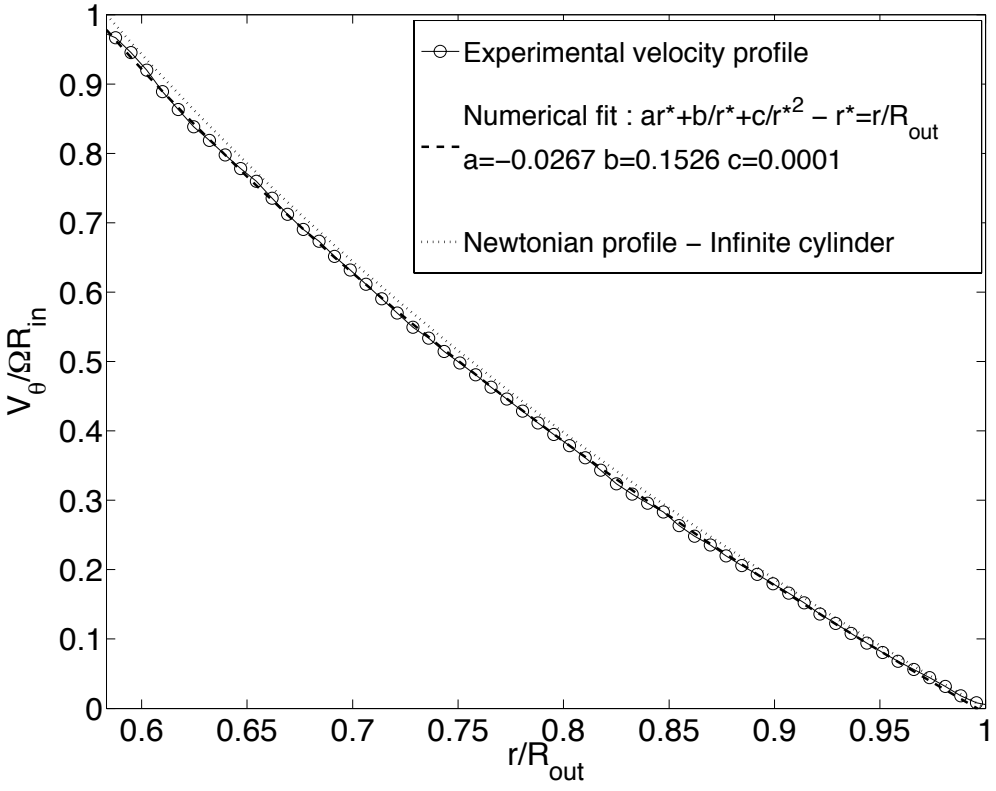

Figure 9: Velocity profile in the Newtonian liquid-Height of liquid: h=26.4mm-Laser position: z=14mm above the bottom. Also represented: fitting function and infinite cylinder profile

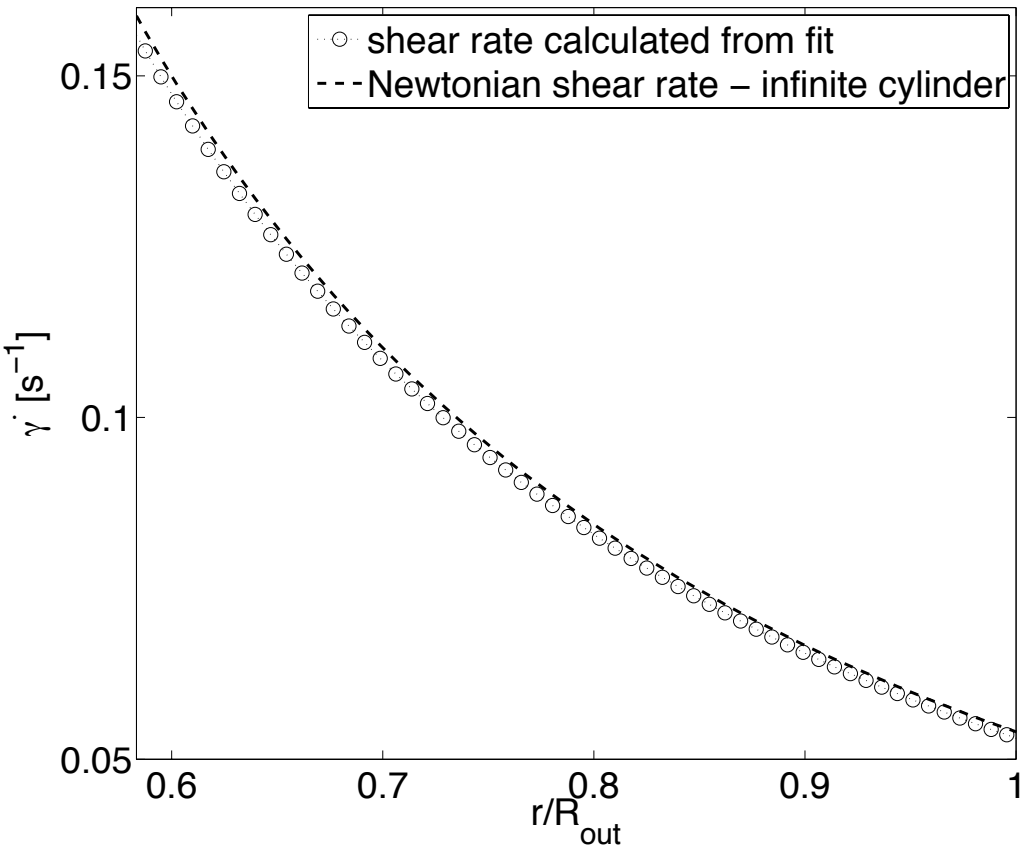

Figure 10: Shear rate profile in the Newtonian liquid-Height of liquid: h=26.4mm-Laser position: z=14mm above the bottom. Also represented: infinite cylinder profile

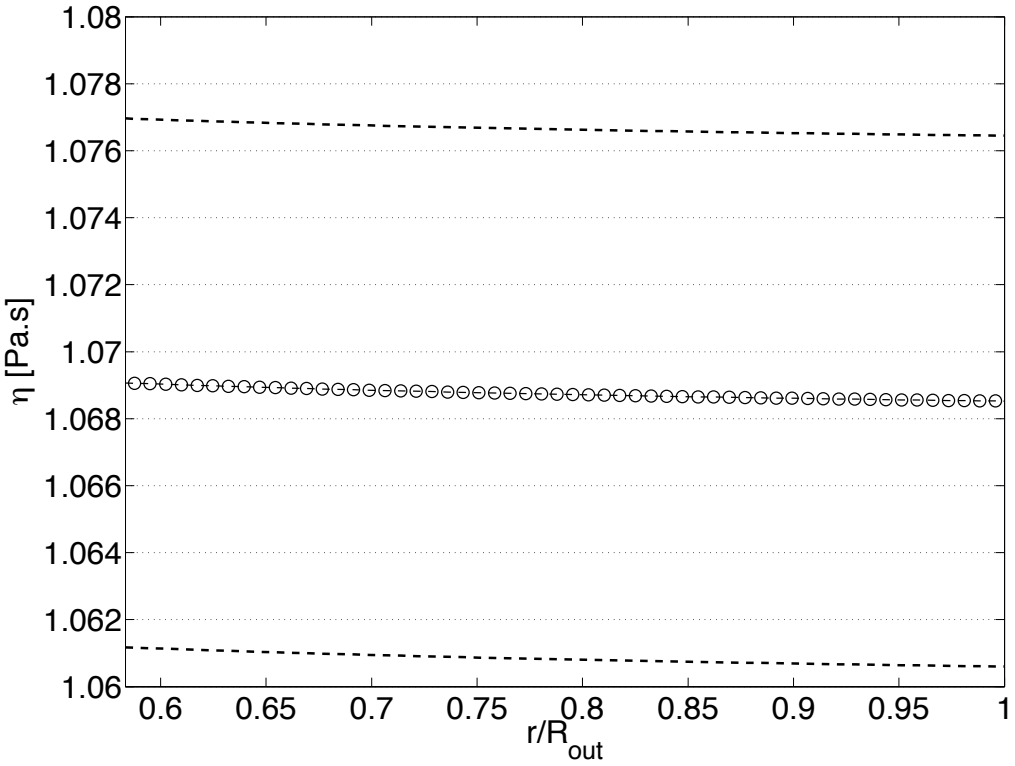

Figure 11: Viscosity profile in the Newtonian liquid-The dashed lines represent the standard error over 80 profiles that is about 1%

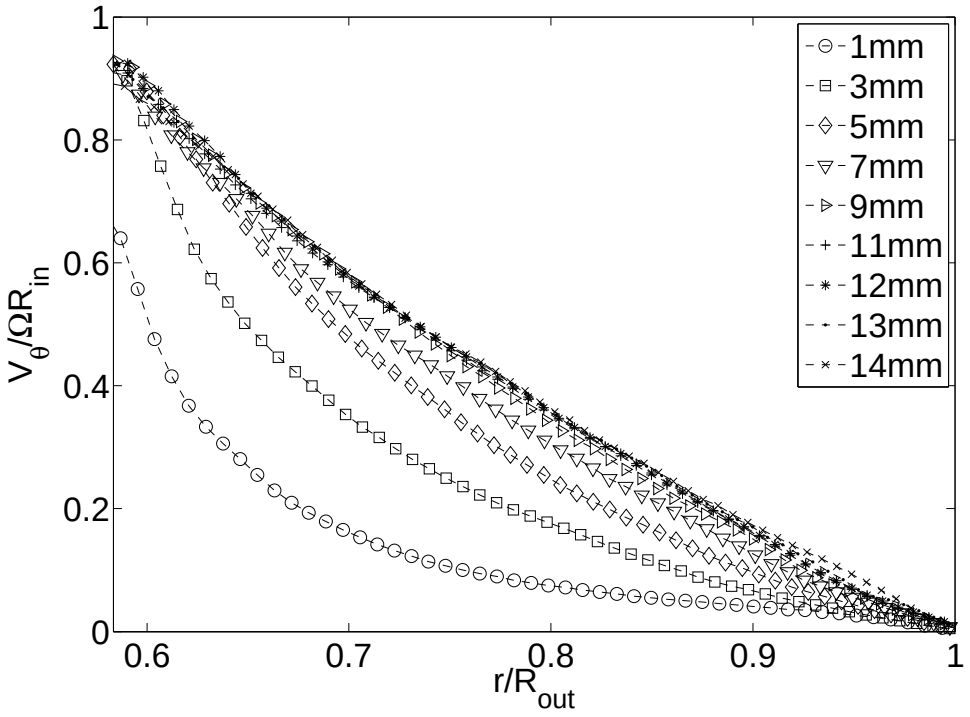

Figure 12: Dimensionless azimuthal velocity profile in a 47% concentrated suspension- The different profiles are determined at different heights from the bottom of the cup. Each profile is the result of an average over 100 instantaneous profiles. Height of the suspension: h=20.1mm.

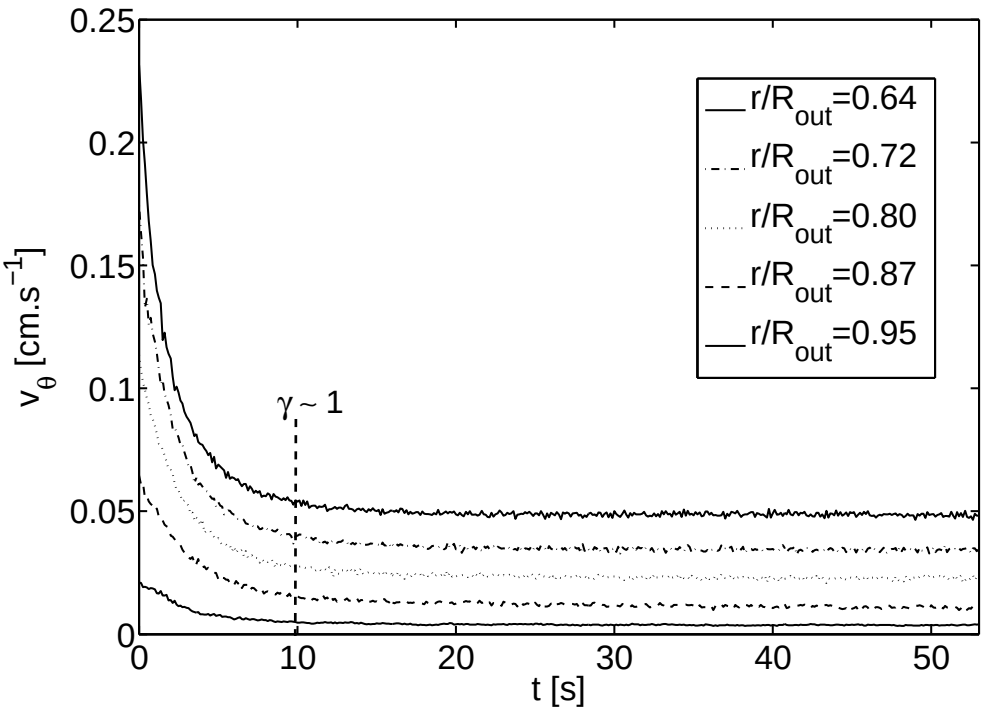

Figure 13: Time evolution of the velocity at various locations in the gap for a 47% concentrated suspension. Height of the suspension: h=45mm. The imposed torque on the inner cylinder is 500μNm and the plateau angular velocity of the bob is 4.4 10^{-2}rad.s^{-1}

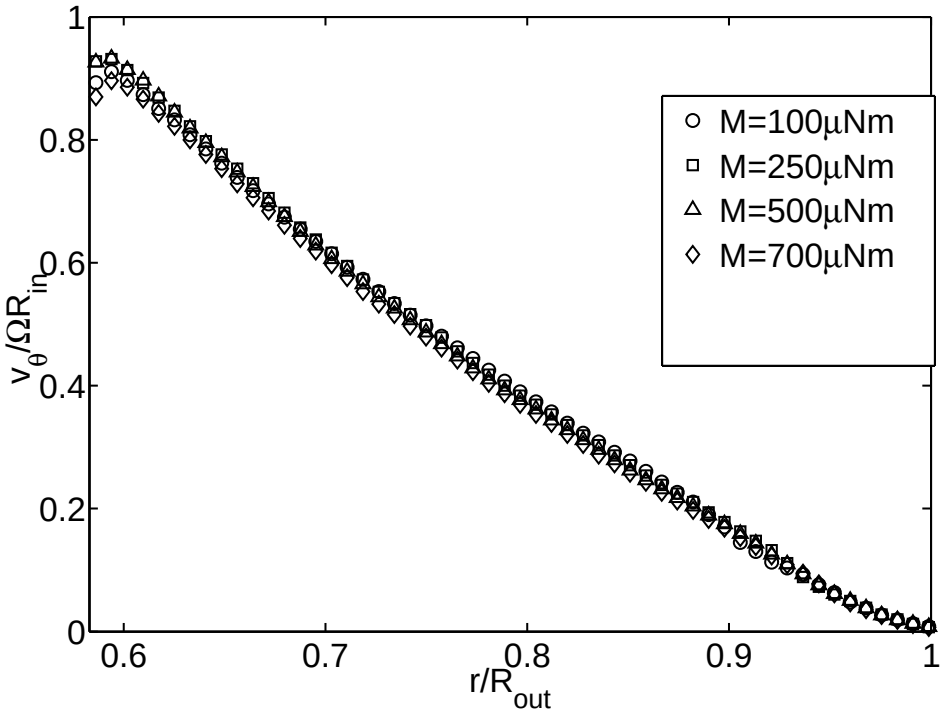

Figure 14: Velocity profiles for different values of the torque for a 47% concentrated suspension. Each profile is the result of an average over 100 instantaneous profiles. Height of the suspension: h=45mm.

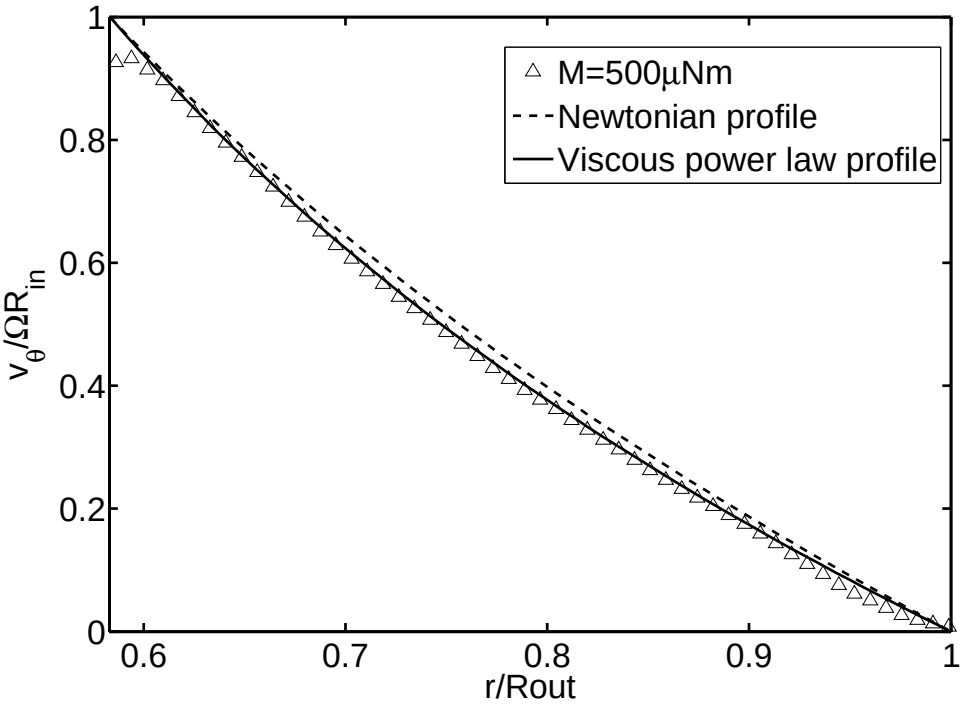

Figure 15: Normalized time averaged azimuthal velocity profile in a 47% concentrated suspension- h=45mm. Dashed line: velocity profile expected for a Newtonian liquid sheared between infinite cylinders. Solid Line: velocity profile deduced from the power law $\sigma_{r\theta} = 40\ \dot{\gamma}^{0.875}$

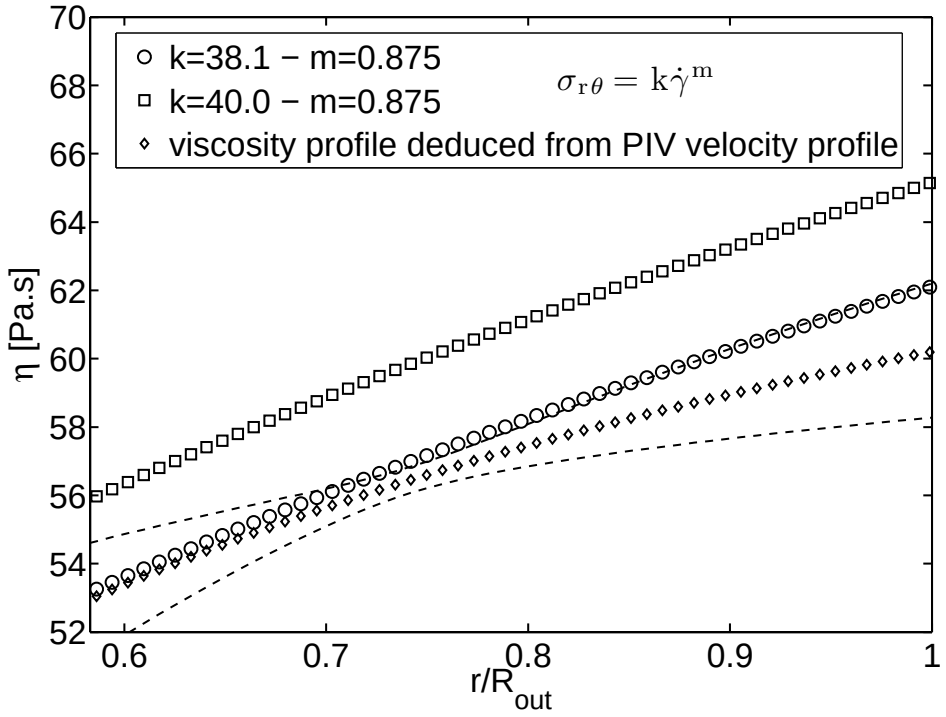

Figure 16: Viscosity profile in a 47% concentrated suspension- Laser position above the bottom of the cup: z=14mm. Height of the suspension h=45mm - The dashed lines represent the standard error over 100 profiles that is at most 4% - $\sigma_{r\theta} = 40\dot{\gamma}^{0.875}$ is the fitting curve to the macroscopic flow curve.

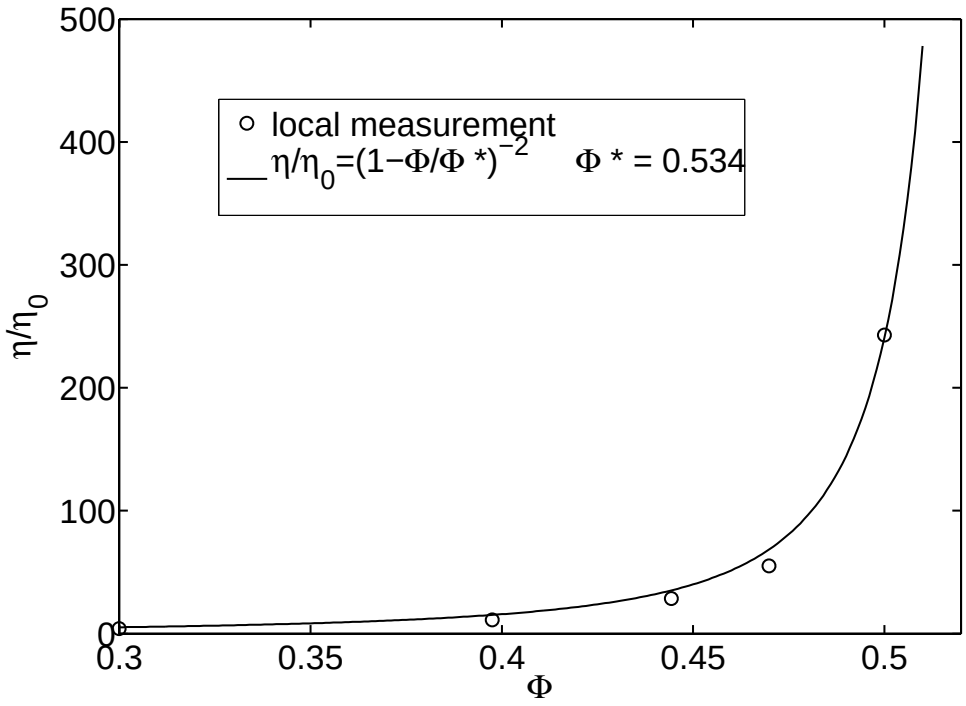

Figure 17: Variation of the relative viscosity deduced from PIV measurements with the particle volume fraction. The measurement has been performed at r=0.77R_{out} and the applied torque has been controlled for the bob angular velocity to be approximately 0.4rpm- Laser position above the bottom of the cup: z=14mm. Height of the suspension h=45mm